INTERNATIONAL JOURNAL FOR NUMERICAL METHODS IN FLUIDS
Int. J. Numer. Meth. Fluids **28**: 337–355 (1998)

MODELLING OF PIPELINE INTEGRITY TAKING INTO ACCOUNT THE FLUID–STRUCTURE INTERACTION

F.B. FREITAS RACHID* AND H.S. COSTA MATTOS

Department of Mechanical Engineering, Universidade Federal Fluminense, 24.210-240 Niterói, RJ, Brasil

SUMMARY

Two mechanical models have been presented in this paper for structural failure prediction of piping systems conveying liquids subjected to pressure transients. One model takes into account the axial fluid–structure interaction (FSI) phenomenon between fluid and pipe motion, whereas the other refers to an extension of the well-known waterhammer formulation. Both models are described by a system of non-linear hyperbolic equations which are solved by using a numerical procedure based upon the operator splitting technique and Glimm's scheme. To implement Glimm's method, it is presented the solution of a 4×4 Riemann problem with discontinuous coefficients. Numerical predictions of both models are presented and compared, so that the influence of the FSI term on the failure analysis is focused on. © 1998 John Wiley & Sons, Ltd.

KEY WORDS: pipeline integrity; fluid–structure interaction; Glimm's scheme; Riemann problem

1. INTRODUCTION

Liquid transmission lines may be subjected to severe pressure loadings during unexpected unsteady flow regimes. Depending on pressure surge magnitudes, temperature operating conditions and piping stiffness, metallic pipes may experience significant inelastic deformations. On the other hand, it is well-known that excessive inelastic strain is one of the mechanisms responsible for degradation of metallic materials. Thus, a reliable design of pipings conveying liquids must take a structural failure analysis into account.

To predict the structural integrity of such piping systems, the classical waterhammer theory has recently been extended to incorporate the damageable inelastic behaviors of the pipe walls [1–3]. The irreversible degradation process of the pipe walls has been included in the pipe material mechanical behavior by means of a continuum damage approach. These works consider the response in the circumferential direction, but neglect any coupling mechanism between fluid and pipe motions. Since experimental and analytical works have shown that, in many practical situations, the uncoupled waterhammer analysis underestimates transient pressure peaks in linear elastic and viscoplastic tubing [4,5], questions arise as to its suitability for predicting the integrity of non-linear inelastic piping.

This paper presents a coupled fluid–structure interaction (FSI) analysis in damageable inelastic tubes to predict structural integrity of pipe walls. The set of non-linear hyperbolic

* Correspondence to: Department of Mechanical Engineering, Universidade Federal Fluminense, 24.210-240 Niterói, RJ, Brasil.

CCC 0271–2091/98/120337–19$17.50
© 1998 John Wiley & Sons, Ltd.
Received February 1997
Revised September 1997

differential equations describing the dynamics of the liquid and the pipe motions are coupled and solved by using a suitable numerical procedure, based upon the operator splitting technique and Glimm's scheme. To implement Glimm's scheme, a closed form solution of a Riemann problem with discontinuous coefficients for a 4×4 system of equations is presented. The mechanical model and numerical procedure are then employed to investigate the influence of the axial FSI on the integrity analysis of pipelines conveying liquids subjected to pressure transients. To achieve this goal, numerical results based on the coupled and uncoupled transient models are compared for a specific piping arrangement.

2. GOVERNING EQUATIONS

In the next paragraphs, the equations of the coupled and uncoupled models will be presented. First, the balance, and then the constitutive equations are presented.

2.1. Balance equations

Piping systems used for liquid transmission are composed of slender members, therefore, pressure transients in fluid-filled compliant pipes are commonly described by means of longitudinal wave theories [6]. Consider an inviscid transient one-dimensional compressible flow confined into a thin-walled pipe (inside radius R and wall thickness e) for which both fluid and pipe wall motions are relevant. Under these assumptions, the balance equations of mass and momentum for horizontal fluid flow in Eulerian co-ordinates are

$$\frac{\partial}{\partial t}(\varphi A) + \frac{\partial}{\partial x}(\varphi A v) = 0, \tag{1.1}$$

$$\frac{\partial}{\partial t}(\varphi A v) + \frac{\partial}{\partial x}(\varphi A v^2) + A\frac{\partial P}{\partial x} = 0. \tag{1.2}$$

In the above equations, P, v, φ and A are functions of the spatial position x along the pipe and the time t. They represent the fluid pressure, the axial fluid velocity, the fluid density and the cross-sectional area of fluid flow, respectively.

The underlying assumptions of small deformations and axisymmetrical plane stress distribution in the pipe wall are assumed to hold for the pipe, so that its motion is described by the following momentum equations (in the axial and radial directions) as

$$\varphi_t \frac{\partial \dot{u}}{\partial t} - \frac{\partial \sigma_x}{\partial x} = 0, \tag{2.1}$$

$$\varphi_t Re \frac{\partial \dot{w}}{\partial t} - RP + \sigma_\theta e = 0, \tag{2.2}$$

together with the strain displacement relationships $\varepsilon = \partial u/\partial x$ and $\varepsilon_\theta = w/R$. In these equations, the non-vanishing stress components (σ_x and σ_θ) and the pipe wall displacements (u and v) in the axial and circumferential directions are functions of x and t, while φ_t designates the pipe density.

To fully couple the fluid and pipe problems, the kinematic relationship between cross-sectional area variations and pipe wall deformations must be imposed. Also, it is necessary to specify an equation of state for the fluid. Neglecting pipe wall ovalization, the cross-sectional area is related to the pipe wall deformation by $A = A_f(1 + \varepsilon_\theta)^2$, whereas the equation of state

© 1998 John Wiley & Sons, Ltd.

for the liquid is, neglecting entropy variation, $\varphi = \varphi_f \exp(P/K)$. Here, K stands for the isoentropic bulk modulus of the liquid (assumed to be constant) and the subscript f is used to designate the undisturbed state from which variations in A and ρ are measured.

If, apart from the small deformation assumption ($\varepsilon_\theta \ll 1$), only slightly compressible fluid flows ($P/K \ll 1$) are admitted, the expressions for A and φ can be linearized and the term φA approximated by

$$\varphi A = \varphi_f A_f(1 + P/K + 2\varepsilon_\theta). \tag{3}$$

Equations (1)–(3) form the balance equations for the problem. The constitutive assumptions which will describe the mechanical behavior of the pipe material must be added to these.

2.2. Constitutive equations

The constitutive theory used in this work has been widely used in several applications and is derived from a general internal variable theory [7]. It encompasses a great number of constitutive relations for damageable inelastic solids and allows the description of different mechanical responses (elastic, plastic, viscoplastic, etc.). In short, the theory is developed by associating state variables with the different dissipative mechanisms involved in the deformation process.

For the isothermal evolution of an inelastic damageable solid under small deformations, it is assumed that its mechanical state is characterized by the set of state variables $(\boldsymbol{\varepsilon}, \boldsymbol{\varepsilon}^a, D, \boldsymbol{\beta})$. $\boldsymbol{\varepsilon}$ is the total strain tensor, $\boldsymbol{\varepsilon}^a$ is the inelastic strain tensor. The scalar variable $D \in [0, 1]$ is the isotropic damage which can be interpreted as a local measure of the degradation of the material induced by deformation. If $D = 0$, the material is virgin and if $D = 1$ the material locally looses its mechanical strength. In practice, for the sake of security, the local failure is considered when the variable D reaches a critical value D_{cr} such that $0 < D_{\text{cr}} < 1$. The variable $\boldsymbol{\beta}$ is associated with the irreversible changes of the internal state of the material. Here, for the specific case of the elasto-viscoplastic behavior $\boldsymbol{\beta} = (p, \boldsymbol{c})$ represents a set of two internal variables p and $\boldsymbol{c}$ related to the isotropic and kinematic hardening phenomena, respectively. It then follows that a complete set of constitutive equations for damageable materials is given by

$$\boldsymbol{\sigma} = (1 - D)\mathbf{C}(\boldsymbol{\varepsilon} - \boldsymbol{\varepsilon}^a), \tag{4.1}$$

$$\dot{\boldsymbol{\varepsilon}}^a = \mathbf{g}, \tag{4.2}$$

$$\dot{D} = h, \tag{4.3}$$

$$\dot{\boldsymbol{\beta}} = \ell, \tag{4.4}$$

where the superimposed dot stands for partial derivative with respect to time and $\mathbf{g}$, h and ℓ are generic functions of the arguments $(\boldsymbol{\sigma}, \boldsymbol{\varepsilon}^a, D, \boldsymbol{\beta})$. The specific forms of these functions for the damageable elasto-viscoplastic behavior are presented in the Appendix.

Equations (4.2)–(4.4) are the evolution equations for the internal variables $\boldsymbol{\varepsilon}^a$, D and $\boldsymbol{\beta}$. In equation (4.1), $\boldsymbol{\sigma}$ is the stress tensor and $\mathbf{C}$ is the classical symmetric fourth-order positive definite tensor of elasticity. If the elastic behavior is isotropic, then

$$\mathbf{C} = \frac{vE}{(1 - 2v)(1 + v)}\,\mathbf{1}_2 \otimes \mathbf{1}_2 + \frac{E}{(1 + v)}\,\mathbf{1}_4,$$

where E and v stand for the Young's modulus and Poisson's ratio, whereas $\mathbf{1}_2$ and $\mathbf{1}_4$ represent the rank two and rank four identity tensors, respectively.

© 1998 John Wiley & Sons, Ltd.

In the particular case of a thin-walled pipe under a plane stress state, σ_x and σ_θ stand for the principal stresses. Only two independent components are associated with them, ε_x^a and ε_θ^a of the inelastic strain tensor $\boldsymbol{\varepsilon}^a$. In addition, if the elastic behavior of the pipe material is assumed to be isotropic, then the constitutive equations can be reduced to

$$\sigma_x = \frac{E(1-D)}{(1-\nu^2)}\{\varepsilon_x + \nu\varepsilon_\theta - \varepsilon_x^a - \nu\varepsilon_\theta^a\}, \tag{5.1}$$

$$\sigma_\theta = \frac{E(1-D)}{(1-\nu^2)}\{\varepsilon_\theta + \nu\varepsilon_x - \varepsilon_\theta^a - \nu\varepsilon_x^a\}, \tag{5.2}$$

$$\dot{\varepsilon}_x^a = g_x, \tag{6.1}$$

$$\dot{\varepsilon}_\theta^a = g_\theta, \tag{6.2}$$

$$\dot{D} = h, \tag{6.3}$$

$$\dot{\boldsymbol{\beta}} = \boldsymbol{\ell}, \tag{6.4}$$

where g_x, g_θ, h and $\boldsymbol{\ell}$ are functions of the arguments $(\sigma_x, \sigma_\theta, \varepsilon_x^a, \varepsilon_\theta^a, D, \boldsymbol{\beta})$.

2.3. Coupled and uncoupled models

In this section, two models (coupled and uncoupled) are derived by combining the basic and constitutive equations. The uncoupled model is an extension of the classical waterhammer theory, in which pipe wall mechanical behavior is accounted for in the circumferential direction only. In addition to this, the coupled model takes the axial FSI between fluid and pipe motions into account. The uncoupled model can be considered a particular case of the coupled model, therefore, we shall start by presenting the last one.

By combining equations (1)–(3) along with (5) and (6), a system of ten equations is obtained for the unknowns $(P, v, u, w, \sigma_x, \sigma_\theta, \varepsilon_x^a, \varepsilon_\theta^a, D, \boldsymbol{\beta})$. For many practical situations, however, it has been shown [8] that the radial pipe wall inertia term in Equation (2.2) might be neglected. In this case, $\sigma_\theta = (RP)/e$ and the system of equations can be reduced to eight equations and eight unknowns because w can be eliminated from the system.

After performing some algebraic manipulations in Equation (5) and changing the variables (P, σ_x) by (ψ, ϕ), according to

$$\psi = \left(\frac{1}{K^*} + \frac{2Rv^2}{eE(1-D)}\right)P - \frac{2v}{E(1-D)}\sigma_x, \tag{7.1}$$

$$\phi = \frac{Rv}{eE(1-D)}P - \frac{1}{E(1-D)}\sigma_x, \tag{7.2}$$

the system of equations for the unknowns $(\psi, v, \dot{u}, \phi, \varepsilon_x^a, \varepsilon_\theta^a, D, \boldsymbol{\beta})$ is obtained as a function of the distance $x \in [0, L]$ along the pipe and time $t \in [0, T]$, as

$$\frac{\partial}{\partial t}(1 + \psi + 2\varepsilon_\theta^a) + \frac{\partial}{\partial x}((1 + \psi + 2\varepsilon_\theta^a)v) = 0, \tag{8.1}$$

$$\frac{\partial}{\partial t}((1 + \psi + 2\varepsilon_\theta^a)v) + \frac{\partial}{\partial x}((1 + \psi + 2\varepsilon_\theta^a)v^2 + c_f^2(\psi - 2v\phi)) = 0, \tag{8.2}$$

$$\frac{\partial \dot{u}}{\partial t} + \frac{\partial}{\partial x}(c_t^2\phi + c_f^2\xi v(2v\phi - \psi)) = 0, \tag{8.3}$$

© 1998 John Wiley & Sons, Ltd.

$$\frac{\partial}{\partial t}(\phi - \varepsilon_x^a) + \frac{\partial \dot{u}}{\partial x} = 0, \tag{8.4}$$

$$\frac{\partial \varepsilon_x^a}{\partial t} = g_x(\psi, \phi, \varepsilon_x^a, \varepsilon_\theta^a, D, \boldsymbol{\beta}), \tag{8.5}$$

$$\frac{\partial \varepsilon_\theta^a}{\partial t} = g_\theta(\psi, \phi, \varepsilon_x^a, \varepsilon_\theta^a, D, \boldsymbol{\beta}), \tag{8.6}$$

$$\frac{\partial D}{\partial t} = h(\psi, \phi, \varepsilon_x^a, \varepsilon_\theta^a, D, \boldsymbol{\beta}), \tag{8.7}$$

$$\frac{\partial \boldsymbol{\beta}}{\partial t} = \ell(\psi, \phi, \varepsilon_x^a, \varepsilon_\theta^a, D, \boldsymbol{\beta}), \tag{8.8}$$

where $c_f = c_f(D)$, $c_t = c_t(D)$ and ξ are given by

$$c_f^2 = K^*/\varphi_f, \qquad c_t^2 = (E(1-D))/\varphi_t, \qquad \xi = (R\varphi_f)/(e\varphi_t),$$

with

$$K^* = K \Big/ \left(1 + \frac{(2RK(1-v^2))}{eE(1-D)}\right).$$

For simplicity, the notation has been simplified by maintaining the same letters to designate the functions g_x, g_θ, h and ℓ, although their arguments have been changed due to Equation (7).

The coupled model presented before admits a further simplification when the low Mach number assumption is taken into account. As shown previously [9], although $M \to \infty$ as $D \to 1$ ($M = (v/c_f)$ is the Mach number), the low Mach number assumption can still be employed if metallic tubes are considered. With this additional hypothesis, the convective terms of Equations (8.1) and (8.2) can be neglected, rendering the following system of equations in the appropriate form of conservation law,

$$\frac{\partial \mathbf{U}}{\partial t} + \frac{\partial}{\partial x}(\mathbf{F}(\mathbf{U})) - \mathbf{W}(\mathbf{U}) = \mathbf{0}. \tag{9}$$

In the above equation, $\mathbf{U} \in \mathbb{R}^8$, $\mathbf{U} = (\psi, v, \dot{u}, \phi, \varepsilon_x^a, \varepsilon_\theta^a, D, \boldsymbol{\beta})^T$, is the conserved quantity, $\mathbf{F}(\mathbf{U}) = \mathbf{F}$: $\mathbb{R}^8 \to \mathbb{R}^8$ and $\mathbf{W}(\mathbf{U}) = \mathbf{W}$: $\mathbb{R}^8 \to \mathbb{R}^8$ represent, respectively, the flux and source/sink terms, which have the form $\mathbf{F} = (v, c_f^2(\psi - 2v\phi), c_t^2 \xi v(2v\phi - \psi), \dot{u}, 0, 0, 0, 0)^T$, $\mathbf{W} = (-g_\theta, 0, 0, g_x, g_x, g_\theta, h, \ell)^T$.

The $\mathbf{W}$ term congregates the evolution equations, which are described by the generic functions g_x, g_θ, h and ℓ.

The pressure transient model characterized by Equation (9), along with the associated particular forms of $\mathbf{U}$, $\mathbf{F}$ and $\mathbf{W}$, is a coupled fluid–structure model, because it not only accounts for the existence but also the interaction of axial pressure waves in fluid flow and axial stress waves in the pipe wall. It can be seen from the $\mathbf{F}$ components that the main coupling mechanism of these waves is due to the Poisson's ratio v. Artificially setting $v = 0$ in $\mathbf{F}$, the equations that describe the fluid and pipe motions are decoupled. A simpler model which does not take stress waves in the pipe wall into account will be considered next.

The uncoupled pressure transient model presented below is a particular case of the previous model. Starting from the coupled model, the uncoupled one is obtained when the axial momentum equation for the pipe wall is disregarded. In such a case, however, it becomes necessary to admit a uniform axial distribution of either stress or strain in advance.

© 1998 John Wiley & Sons, Ltd.

The two most important cases arise when it is assumed that either $\sigma_x = 0$ (case a) or $\varepsilon_x = 0 = \varepsilon_x^a$ (case b) throughout the pipe. These two cases represent typical pipe support situations in which either the pipe is anchored with expansion joints or it is anchored throughout against axial movement [6]. Unlike the coupled model, in both cases only one independent stress component ($\sigma_\theta = RP/e$) will exist. Although representing different physical situations, the cases can be described by the same set of equations and in the same form as Equation (9) if ψ and $c_f = c_f(D)$ are redefined as $\psi = 1 + P/K'$ and $c_f^2 = K'/\varphi_f$. Here, $K' = K/[1 + (2RK\gamma)/(eE(1-D))]$, where $\gamma = 1$ if case (a) is considered, or $\gamma = 1 - \nu^2$ if case (b) is considered. Now, the quantity $\mathbf{U} \in \mathbb{R}^6$, $\mathbf{U} = (\psi, v, \varepsilon_x^a, \varepsilon_\theta^a, D, \beta)^T$ and the particular forms of $\mathbf{F}$ and $\mathbf{W}$ are given by $\mathbf{F} = (v, c_f^2\psi, 0, 0, 0, 0)^T$, $\mathbf{W} = (-g_\theta, 0, g_x, h, \ell)^T$.

3. NUMERICAL PROCEDURE

Equation (9) forms a one-dimensional system of non-linear partial differential equations (PDE) of hyperbolic type. In this paper, Glimm's scheme, together with the operator splitting technique, is used to solve Equation (9). Glimm's scheme [10–14], as well as other methods [15] which require the solution of the associated Riemann problem, has been employed to solve such one-dimensional problems because of its proven efficiency in treating discontinuous initial data and capturing solutions which present first- or zeroth-order discontinuities. For the problem considered herein, two specific reasons may be cited for using this numerical approach. The first one is related to the wave propagation velocities $a_f(D)$ and $a_t(D)$ (see Equation (21)) of the problem which may present severe gradients as a consequence of a localized damage evolution induced by inelastic strains. The other is associated with the capability of the method in consistently dealing with a discontinuous initial field of damage. From the physical viewpoint, this situation naturally arises due to initial defects, or when a stretch of a damaged pipe is replaced with another virgin pipe.

3.1. The operator splitting and Glimm's scheme

To obtain a numerical solution for Equation (9), consider a uniform partition $0 = x_1 < \cdots x_i < x_{i+1} < \cdots < x_{N+1} = L$ of the spatial domain $[0, L]$, such that $\Delta x = x_{i+1} - x_i$. The procedure used to advance the solution from time t^n to time $t^{n+1} = t^n + \Delta t$ is based upon the operator splitting technique. With this technique, the approximation for $\mathbf{U}(x, t)$ at time $t = t^{n+1}$ and $x = x_i$, $\mathbf{U}_i^{n+1}$, is obtained by solving

$$\frac{\partial \mathbf{U}}{\partial t} = \mathbf{W}(\mathbf{U}), \tag{9.1}$$

$$\mathbf{U} = \tilde{\mathbf{U}}^{n+1}(x) \quad \text{at} \quad t = t^n, \tag{9.2}$$

as follows:

$$\mathbf{U}_i^{n+1} = \tilde{\mathbf{U}}_i^{n+1} + \Delta t \mathbf{W}(\tilde{\mathbf{U}}_i^{n+1}). \tag{10}$$

In the above expression, $\mathbf{U}_i^{n+1}$ and $\tilde{\mathbf{U}}_i^{n+1}$ stand for the approximations of $\mathbf{U}(x = x_i, t = t^{n+1})$ and $\tilde{\mathbf{U}}(x = x_i, t = t^{n+1})$, respectively.

The field $\tilde{\mathbf{U}}^{n+1}(x) = \tilde{\mathbf{U}}(x, t = t^{n+1})$, used as the initial condition in Equation (9), is the solution evaluated at time $t = t^{n+1}$ of the homogeneous hyperbolic problem

© 1998 John Wiley & Sons, Ltd.

$$\frac{\partial \tilde{\mathbf{U}}}{\partial t} + \frac{\partial}{\partial x}(\mathbf{F}(\tilde{\mathbf{U}})) = \mathbf{0}, \tag{11.1}$$

$$\tilde{\mathbf{U}} = \mathbf{U}^n(x) \quad \text{at} \quad t = t^n. \tag{11.2}$$

To proceed with the construction of the numerical solution, it is worth noting that the quantity $\tilde{\mathbf{U}} \in \mathbb{R}^8$ and the flux term $\mathbf{F} \in \mathbb{R}^8$ admit the decomposition $\tilde{\mathbf{U}} = ({}^e\tilde{\mathbf{U}}, {}^a\tilde{\mathbf{U}})^T$ and $\mathbf{F} = ({}^e\mathbf{F}, {}^a\mathbf{F})^T$, where ${}^a\tilde{\mathbf{U}}$, ${}^a\mathbf{F}$, ${}^e\tilde{\mathbf{U}}$ and ${}^e\mathbf{F} \in \mathbb{R}^4$ are such that

$${}^e\mathbf{U} = (\psi, v, \dot{u}, \phi)^T,$$

$${}^a\mathbf{U} = (\varepsilon_x^a, \varepsilon_\theta^a, D, \boldsymbol{\beta})^T,$$

$${}^e\mathbf{F} = (v, c_f^2(\psi - 2v\phi), c_i^2\phi + c_f^2\xi v(2v\phi - \psi), \dot{u})^T,$$

$${}^a\mathbf{F} = 0.$$

In view of this, Equation (11) can be rewritten as

$$\frac{\partial {}^e\tilde{\mathbf{U}}}{\partial t} + \frac{\partial}{\partial x}({}^e\mathbf{F}({}^e\tilde{\mathbf{U}}, {}^a\tilde{\mathbf{U}})) = \mathbf{0}, \tag{12.1}$$

$$\frac{\partial {}^a\tilde{\mathbf{U}}}{\partial t} = \mathbf{0}, \tag{12.2}$$

$$\tilde{\mathbf{U}} = ({}^e\mathbf{U}^n(x), {}^a\mathbf{U}^n(x))^T \quad \text{at} \quad t = t^n. \tag{12.3}$$

Equation (12) is solved numerically using Glimm's scheme [16]. As a first step for employing Glimm's scheme, the initial data are assumed to be approximated by piecewise constant functions, as

$$\tilde{\mathbf{U}}(x, t^n) \simeq \mathbf{U}_i^n = ({}^e\mathbf{U}_i^n, {}^a\mathbf{U}_i^n)^T = ({}^e\mathbf{U}(x_i, t^n), {}^a\mathbf{U}(x_i, t^n))^T, \tag{13}$$

for $x \in (a_i, b_i)$ and $1 \le i \le N+1$, where

$$a_i = \begin{cases} x_1, & \text{if } i = 1 \\ x_i - (\Delta x)/2, & \text{if } 1 < i \le N+1 \end{cases},$$

$$b_i = \begin{cases} x_i + (\Delta x)/2, & \text{if } 1 \le i < N+1 \\ x_{N+1}, & \text{if } i = N+1 \end{cases}.$$

The above approximations give rise, for each two consecutive steps i and $i+1$, to an initial value problem known as the Riemann problem, characterized by Equations (12.1) and (12.2), with initial data given by

$$\tilde{\mathbf{U}}(x, t^n) = ({}^e\tilde{\mathbf{U}}, {}^a\tilde{\mathbf{U}})^T(x, t^n) = \begin{cases} ({}^e\mathbf{U}_i^n, {}^a\mathbf{U}_i^n)^T & \text{for } -\infty < x < x_i + \dfrac{\Delta x}{2} \\ ({}^e\mathbf{U}_{i+1}^n, {}^a\mathbf{U}_{i+1}^n)^T & \text{for } x_{i+1} - \dfrac{\Delta x}{2} < x < \infty \end{cases}, \tag{14}$$

$\hat{\mathbf{U}}(x, t) = ({}^e\hat{\mathbf{U}}(\zeta), {}^a\hat{\mathbf{U}}(\zeta))^T$ denotes the generalized solution of Equation (12.1), (12.2) and (14), with $\zeta = (x - (x_i + 0.5\Delta x))/(t - t^n)$, ${}^e\hat{\mathbf{U}}(\zeta)$given by Equation (25) and ${}^a\hat{\mathbf{U}}(\zeta)$ given by

$${}^a\hat{\mathbf{U}}(\zeta) = \begin{cases} {}^a\mathbf{U}_i^n, & \text{if } \zeta < 0 \\ {}^a\mathbf{U}_{i+1}^n, & \text{if } \zeta > 0 \end{cases},$$

© 1998 John Wiley & Sons, Ltd.

Glimm's approximation for Equation (11) (or (12)) at time t^{n+1} is obtained by introducing a sequence of equidistributed random numbers $\{\theta_n\}$, $\theta_n \in (0, 1)$, so that

$$\tilde{\mathbf{U}}^{n+1}(x) \simeq \tilde{\mathbf{U}}_j^{n+1} = \hat{\mathbf{U}}(x = x_i + \theta_n \Delta x, t = t^{n+1}), \tag{15}$$

for $x \in (a_i, b_i)$ and $1 \leq i \leq N$, with j defined by

$$j = \begin{cases} i, & \text{if } \theta_n \leq 1/2 \\ i+1, & \text{if } \theta_n > 1/2 \end{cases}.$$

In the procedure, the time instant t^{n+1} must be such that the Courant–Friedrichs–Levy condition [16] is satisfied, i.e.

$$t^{n+1} - t^n = \Delta t \leq \frac{\Delta x}{2|\lambda|_{\max}}, \tag{16}$$

where $|\lambda|_{\max}$ is the maximum (in absolute value) propagation speed, taking into account the N Riemann problems at time t^n.

The procedure can be repeated throughout until a desired time of simulation has been reached or the damage variable has reached its critical value D_{cr}. Convergence features of Glimm's scheme, which is first-order-accurate in time, can be found in Chapter 19 of Reference [16].

3.2. The associated Riemann problem

The Riemann problem (centered at $x = x_0$) associated with Equation (12) is an initial value problem of the form [16]

$$\frac{\partial {}^e\tilde{\mathbf{U}}}{\partial t} + \frac{\partial}{\partial x}({}^e\bar{\bar{\mathbf{F}}}({}^e\tilde{\mathbf{U}}, x)) = \mathbf{0}, \tag{17.1}$$

$${}^e\tilde{\mathbf{U}}(x, t = t_o) = \begin{cases} {}^e\mathbf{U}_{\text{L}} & \text{if } x < x_o \\ {}^e\mathbf{U}_{\text{R}} & \text{if } x > x_o \end{cases}, \tag{17.2}$$

with discontinuous coefficients c_f and c_t, such that

$$(c_f, c_t) = \begin{cases} ((c_f)_{\text{L}}, (c_t)_{\text{L}}) = (c_f(D_{\text{L}}), c_t(D_{\text{L}})) = \text{constants} & \text{if } x < x_o \\ ((c_f)_{\text{R}}, (c_t)_{\text{R}}) = (c_f(D_{\text{R}}), c_t(D_{\text{R}})) = \text{constants} & \text{if } x > x_o \end{cases}. \tag{17.3}$$

In the above expressions, ${}^e\mathbf{U}_{\text{L}} = (\psi_{\text{L}}, v_{\text{L}}, \dot{u}_{\text{L}}, \phi_{\text{L}})^T$ and ${}^e\mathbf{U}_{\text{R}} = (\psi_{\text{R}}, v_{\text{R}}, \dot{u}_{\text{R}}, \phi_{\text{R}})^T$ are arbitrary constant states, D_{L} and D_{R} are arbitrary constants, which are all defined at the left and at the right of $x = x_o$ and at $t = t_o$. With relation to the scheme presented in Section 3.1, x_o and t_o refer to the position $x_i + 0.5\Delta x$ and the time instant t^n, respectively.

The above problem is classified in the literature as a generalized Riemann problem because the flux term depends on x. In this case, such a dependence arises due to the splitting adopted in Section 3.1, along with the dependence on D of the coefficients $c_f = c_f(D)$ and $c_t = c_t(D)$ which are present in ${}^e\mathbf{F}$.

The flux function ${}^e\bar{\bar{\mathbf{F}}}({}^e\tilde{\mathbf{U}}, x)$ has a sharp discontinuity at $x = x_o$ and is independent of x for $x < x_o$ and $x > x_o$. Moreover, it is linear on ${}^e\tilde{\mathbf{U}}$ so that the function ${}^e\bar{\bar{\mathbf{F}}}$ can be redefined with another function, ${}^e\bar{\mathbf{F}}$: $\mathbb{R}^4 \to \mathbb{R}^4$, such that

$${}^e\bar{\bar{\mathbf{F}}}({}^e\tilde{\mathbf{U}}, x) = {}^e\bar{\mathbf{F}}({}^e\tilde{\mathbf{U}}) = \begin{cases} \mathbf{A}_{\text{L}}\,{}^e\tilde{\mathbf{U}} & \text{for } x < x_o \\ \mathbf{A}_{\text{R}}\,{}^e\tilde{\mathbf{U}} & \text{for } x > x_o \end{cases}, \tag{18}$$

where $\mathbf{A}_{\text{L}} = \mathbf{A}((c_f)_{\text{L}}, (c_t)_{\text{L}})$ and $\mathbf{A}_{\text{R}} = \mathbf{A}((c_f)_{\text{R}}, (c_t)_{\text{R}})$.

© 1998 John Wiley & Sons, Ltd.

In the above expressions, $\mathbf{A} = \mathbf{A}(c_f, c_t) \in \mathbb{R}^{4\times 4}$ is the Jacobian matrix $\mathbf{A} = \mathrm{d}^e\bar{\mathbf{F}}/\mathrm{d}^e\tilde{\mathbf{U}}$, which is given by

$$\mathbf{A} = \begin{bmatrix} 0 & 1 & 0 & 0 \\ c_f^2 & 0 & 0 & -2v \\ \xi c_f^2 & 0 & 0 & c_t^2 - 2v^2\xi c_f^2 \\ 0 & 0 & 1 & 0 \end{bmatrix}.$$

Equation (17) is invariant under the scale transformation $x' = \alpha(x - x_o)$ and $t' = \alpha(t - t_o)$, $\alpha > 0$, therefore, its solution depends only on the ratio $\zeta = (x - x_o)/(t - t_o)$. In other words, it is of the form ${}^e\tilde{\mathbf{U}}(x, t) = {}^e\hat{\mathbf{U}}(\zeta)$, $t > t_o$, where ${}^e\hat{\mathbf{U}}$: $\mathbb{R} \to \mathbb{R}^4$ is a piecewise continuous function. For simplicity and without losing generality it is now assumed that $x_o = 0$ and $t_o = 0$.

The (generalized) solution of this particular problem is constructed by connecting the left state ${}^e\mathbf{U}_\mathrm{L}$ to the right state ${}^e\mathbf{U}_\mathrm{R}$ through intermediate states which should be determined. Due to the linearity of ${}^e\bar{\mathbf{F}}$, these states must be connected by shocks waves (contact discontinuities). Each shock must satisfy the Rankine–Hugoniot jump condition [16], expressed as

$$s[{}^e\tilde{\mathbf{U}}] = [{}^e\bar{\mathbf{F}}({}^e\bar{\mathbf{U}})], \tag{19}$$

where $[\chi]$ represents the jump of χ across adjacent states and s stands for the propagation speed of the shock.

For either $\zeta < 0$ or $\zeta > 0$, Equation (19) gives

$$(\mathbf{A} - s\mathbf{1})[{}^e\tilde{\mathbf{U}}] = \mathbf{0}. \tag{20}$$

$[{}^e\tilde{\mathbf{U}}] \neq 0$, therefore, it follows that s is the eigenvalue of $\mathbf{A}$, $s = \lambda_i$ $(i = 1, \ldots, 4)$, which are (in crescent order)

$$\lambda_1 = -a_t < -a_f = \lambda_2 < 0 < \lambda_3 = a_f < a_t = \lambda_4, \tag{21}$$

where $a_t = \bar{a}_t(c_f, c_t) = a_t(D)$ and $a_f = \bar{a}_f(c_f, c_t) = a_f(D)$ are given by

$$a_t = \left\{\frac{1}{2}(\omega^2 + (\omega^4 - 4c_f^2c_t^2)^{1/2})\right\}^{1/2}, \qquad a_f = \left\{\frac{1}{2}(\omega^2 - (\omega^4 - 4c_f^2c_t^2)^{1/2})\right\}^{1/2},$$

with $\omega^2 = c_f^2 + c_t^2 + 2v^2\xi c_f^2$.

For $\zeta < 0$, $(\mathbf{A}_\mathrm{L} - \mathrm{s}\mathbf{1})[{}^e\tilde{\mathbf{U}}] = \mathbf{0}$ implies $s = -(a_t)_\mathrm{L} < 0$ or $s = -(a_f)_\mathrm{L} < 0$. On the other hand, for $\zeta > 0$, $(\mathbf{A}_\mathrm{R} - \mathrm{s}\mathbf{1})[{}^e\tilde{\mathbf{U}}] = \mathbf{0}$ implies $s = (a_f)_\mathrm{R} > 0$ or $s = (a_t)_\mathrm{R} > 0$, where

$$(a_t)_\mathrm{L} = \bar{a}_t((c_f)_\mathrm{L}, (c_t)_\mathrm{L}) = a_t(D_\mathrm{L}), \qquad (a_t)_\mathrm{R} = \bar{a}_t((c_f)_\mathrm{R}, (c_t)_\mathrm{R}) = a_t(D_\mathrm{R}),$$

$$(a_f)_\mathrm{L} = \bar{a}_f((c_f)_\mathrm{L}, (c_t)_\mathrm{L}) = a_f(D_\mathrm{L}), \qquad (a_f)_\mathrm{R} = \bar{a}_f((c_f)_\mathrm{R}, (c_t)_\mathrm{R}) = a_f(D_\mathrm{R}).$$

For both $\zeta < 0$ and $\zeta > 0$, s corresponds to the eigenvalues λ_i $(i = 1, \ldots, 4)$, in the respective regions of the x–t plane. Moreover, because $(\mathbf{A} - s\mathbf{1})$ has rank equal to three for every $s = \lambda_i$ $(i = 1, \ldots, 4)$, the dependent line can be eliminated and Equation (20) can be written as

$$\mathbf{B}[{}^e\tilde{\mathbf{U}}] = \mathbf{0}, \tag{22}$$

where $\mathbf{B} = \mathbf{B}(c_f, s) \in \mathbb{R}^{3\times 4}$ has the form

© 1998 John Wiley & Sons, Ltd.

$$\mathbf{B} = \begin{bmatrix} s & -1 & 0 & 0 \\ 0 & (s^2 - c_f^2) & 2vc_f^2 & 0 \\ 0 & 0 & -1 & 0 \end{bmatrix}.$$

$a_t(D) > a_f(D)$, therefore, for all $D \in [0, 1)$, the solution of the problem is constructed by connecting the left state ${}^e\mathbf{U}_\mathrm{L}$ to an intermediate state ${}^e\mathbf{U}_\mathrm{L}^*$, with the shock speed $s = -(a_t)_\mathrm{L}$ (see Figure 1);

$${}^e\mathbf{U}_\mathrm{L} \xrightarrow{s=-(a_t)_\mathrm{L}} {}^e\mathbf{U}_\mathrm{L}^* \Rightarrow \mathbf{B}((c_f)_\mathrm{L}, s = -(a_t)_\mathrm{L})({}^e\mathbf{U}_\mathrm{L} - {}^e\mathbf{U}_\mathrm{L}^*) = \mathbf{0}. \tag{23.1}$$

Another intermediate state ${}^e\mathbf{U}_\mathrm{L}^{**}$ is connected to the state ${}^e\mathbf{U}_\mathrm{L}^*$, with the shock speed $s = -(a_f)_\mathrm{L}$ (see Figure 1);

$${}^e\mathbf{U}_\mathrm{L}^* \xrightarrow{s=-(a_f)_\mathrm{L}} {}^e\mathbf{U}_\mathrm{L}^{**} \Rightarrow \mathbf{B}((c_f)_\mathrm{L}, s = -(a_f)_\mathrm{L})({}^e\mathbf{U}_\mathrm{L}^{**} - {}^e\mathbf{U}_\mathrm{L}^*) = \mathbf{0}. \tag{23.2}$$

Similarly, an intermediate state ${}^e\mathbf{U}_\mathrm{R}^*$ is connected to the right state ${}^e\mathbf{U}_\mathrm{R}$ through the shock speed $s = (a_t)_\mathrm{R}$ (see Figure 1);

$${}^e\mathbf{U}_\mathrm{R}^* \xrightarrow{s=+(a_t)_\mathrm{R}} {}^e\mathbf{U}_\mathrm{R} \Rightarrow \mathbf{B}((c_f)_\mathrm{R}, s = +(a_t)_\mathrm{R})({}^e\mathbf{U}_\mathrm{R} - {}^e\mathbf{U}_\mathrm{R}^*) = \mathbf{0}. \tag{23.3}$$

Finally, the states ${}^e\mathbf{U}_\mathrm{R}^*$ and ${}^e\mathbf{U}_\mathrm{R}^{**}$ are connected with the shock $s = (a_f)_\mathrm{R}$ (see Figure 1);

$${}^e\mathbf{U}_\mathrm{R}^{**} \xrightarrow{s=+(a_f)_\mathrm{R}} {}^e\mathbf{U}_\mathrm{R}^* \Rightarrow \mathbf{B}((c_f)_\mathrm{R}, s = +(a_f)_\mathrm{R})({}^e\mathbf{U}_\mathrm{R}^* - {}^e\mathbf{U}_\mathrm{R}^{**}) = \mathbf{0}. \tag{23.4}$$

To complete the solution, the states ${}^e\mathbf{U}_\mathrm{L}^{**}$ and ${}^e\mathbf{U}_\mathrm{R}^{**}$ must be connected. This is done by imposing a stationary shock (a shock with speed $s = 0$) at $x = 0$ with Equation (19), as illustrated in Figure 1;

$${}^e\mathbf{U}_\mathrm{L}^{**} \xrightarrow{s=0} {}^e\mathbf{U}_\mathrm{R}^{**} \Rightarrow \mathbf{A}_\mathrm{R}{}^e\mathbf{U}_\mathrm{R}^{**} - \mathbf{A}_\mathrm{L}{}^e\mathbf{U}_\mathrm{L}^{**} = \mathbf{0}. \tag{23.5}$$

When Equations (23.1)–(23.5), which connect the states ${}^e\mathbf{U}_\mathrm{L} \to {}^e\mathbf{U}_\mathrm{L}^* \to {}^e\mathbf{U}_\mathrm{L}^{**} \to {}^e\mathbf{U}_\mathrm{R}^{**} \to {}^eU_\mathrm{R}^* \to {}^e\mathbf{U}_\mathrm{R}$ are grouped together, a system of algebraic equations for the unknown $\mathscr{U} = ({}^e\mathbf{U}_\mathrm{L}^*, {}^e\mathbf{U}_\mathrm{L}^{**}, {}^e\mathbf{U}_\mathrm{R}^{**}, {}^e\mathbf{U}_\mathrm{R}^*)^T \in \mathbb{R}^{16}$, ${}^e\mathbf{U}_\mathrm{L}^* = (\psi_\mathrm{L}^*, v_\mathrm{L}^*, \dot{u}_\mathrm{L}^*, \phi_\mathrm{L}^*)^T$, ${}^e\mathbf{U}_\mathrm{L}^{**} = (\psi_\mathrm{L}^{**}, v_\mathrm{L}^{**}, \dot{u}_\mathrm{L}^{**}, \phi_\mathrm{L}^{**})^T$, ${}^e\mathbf{U}_\mathrm{R}^{**} = (\psi_\mathrm{R}^{**}, v_\mathrm{R}^{**}, \dot{u}_\mathrm{R}^{**}, \phi_\mathrm{R}^{**})^T$ and ${}^e\mathbf{U}_\mathrm{R}^* = (\psi_\mathrm{R}^*, v_\mathrm{R}^*, \dot{u}_\mathrm{R}^*, \phi_\mathrm{R}^*)^T$, is obtained as

$$\mathscr{A}\mathscr{U} = \mathscr{B}, \tag{24}$$

where $\mathscr{A} \in \mathbb{R}^{16 \times 16}$ and $\mathscr{B} \in \mathbb{R}^{16}$ are

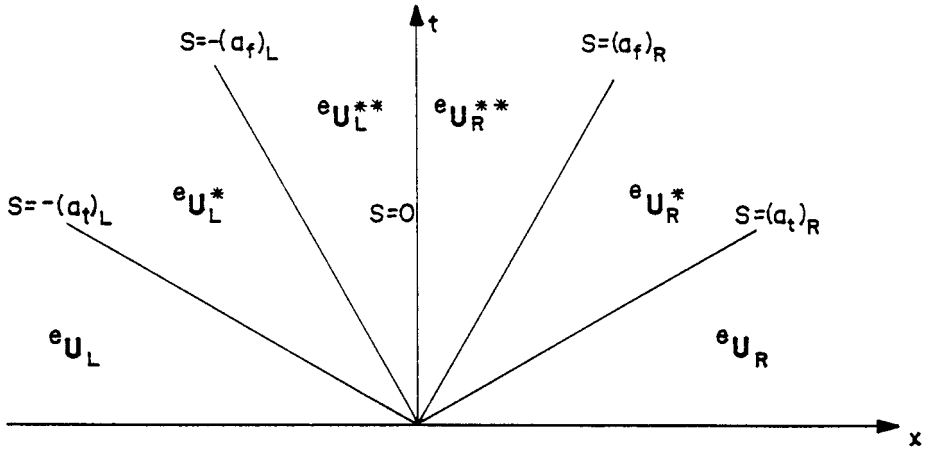

Figure 1. Solution of the Riemann problem in the x–t plane.

© 1998 John Wiley & Sons, Ltd.

$$\mathscr{A} = \begin{bmatrix} \mathbf{B}_{\mathrm{L}}(s = -(a_t)_{\mathrm{L}}) & \mathbf{0}_{3\times 4} & \mathbf{0}_{3\times 4} & \mathbf{0}_{3\times 4} \\ \mathbf{B}_{\mathrm{L}}(s = -(a_f)_{\mathrm{L}}) & -\mathbf{B}_{\mathrm{L}}(s = -(a_f)_{\mathrm{L}}) & \mathbf{0}_{3\times 4} & \mathbf{0}_{3\times 4} \\ \mathbf{0}_{4\times 4} & -\mathbf{A}_{\mathrm{L}} & \mathbf{A}_{\mathrm{R}} & \mathbf{0}_{4\times 4} \\ \mathbf{0}_{3\times 4} & \mathbf{0}_{3\times 4} & -\mathbf{B}_{\mathrm{R}}(s = (a_f)_{\mathrm{R}}) & \mathbf{B}_{\mathrm{R}}(s = (a_f)_{\mathrm{R}}) \\ \mathbf{0}_{3\times 4} & \mathbf{0}_{3\times 4} & \mathbf{0}_{3\times 4} & \mathbf{B}_{\mathrm{R}}(s = (a_t)_{\mathrm{R}}) \end{bmatrix},$$

$$\mathscr{B} = (\mathbf{B}_{\mathrm{L}}(s = -(a_t)_{\mathrm{L}}), \mathbf{0}_3, \mathbf{0}_4, \mathbf{0}_3, \mathbf{B}_{\mathrm{R}}(s = +(a_t)_{\mathrm{R}}))^T.$$

In the above expressions, $\mathbf{B}_{\mathrm{L}}(s) = \mathbf{B}(c_f = (c_f)_{\mathrm{L}}, s)$ and $\mathbf{B}_{\mathrm{R}}(s) = \mathbf{B}(c_f = (c_f)_{\mathrm{R}}, s)$ with $\mathbf{0}_{3\times 4}$, $\mathbf{B}_{\mathrm{L}}$ and $\mathbf{B}_{\mathrm{R}} \in \mathbb{R}^{3\times 4}$ and $\mathbf{0}_{4\times 4}$, $\mathbf{A}_{\mathrm{L}}$ and $\mathbf{A}_{\mathrm{R}} \in \mathbb{R}^{4\times 4}$.

By solving Equation (24), the solution (unique) of the generalized Riemann problem is obtained, no matter how distant are the left and right states, and it is expressed as

$${}^e\hat{\mathbf{U}}(\zeta) = \begin{cases} {}^e\mathbf{U}_{\mathrm{L}}, & \text{for } -\infty < \zeta < s = -(a_t)_{\mathrm{L}} \\ {}^e\mathbf{U}^*_{\mathrm{L}}, & \text{for } s = -(a_t)_{\mathrm{L}} < \zeta < s = -(a_f)_{\mathrm{L}} \\ {}^e\mathbf{U}^{**}_{\mathrm{L}}, & \text{for } s = -(a_f)_{\mathrm{L}} < \zeta < s = 0 \\ {}^e\mathbf{U}^{**}_{\mathrm{R}}, & \text{for } s = 0 < \zeta < s = +(a_f)_{\mathrm{R}} \\ {}^e\mathbf{U}^*_{\mathrm{R}}, & \text{for } s = +(a_f)_{\mathrm{R}} < \zeta < s = +(a_t)_{\mathrm{R}} \\ {}^e\mathbf{U}_{\mathrm{R}}, & \text{for } s = +(a_t)_{\mathrm{R}} < \zeta < +\infty \end{cases}, \tag{25}$$

Figure 1 presents the regions in the x–t plane where the above solution is defined.

With respect to the solution presented before, it is worth mentioning two important features. When, in particular, $D_{\mathrm{L}} = D_{\mathrm{R}}$, the classical Riemann problem is recovered for which $(c_f)_{\mathrm{L}} = (c_f)_{\mathrm{R}} = c_f$, $(c_t)_{\mathrm{L}} = (c_t)_{\mathrm{R}} = c_t$, $(a_f)_{\mathrm{L}} = (a_f)_{\mathrm{R}} = a_f$ and $(a_t)_{\mathrm{L}} = (a_t)_{\mathrm{R}} = a_t$. As a consequence, only three intermediate states will exist ${}^e\mathbf{U}^*_{\mathrm{L}}$, ${}^e\mathbf{U}^{**}$ and ${}^e\mathbf{U}^*_{\mathrm{R}}$, because ${}^e\mathbf{U}^{**}_{\mathrm{L}} = {}^e\mathbf{U}^{**}_{\mathrm{R}} = {}^e\mathbf{U}^{**}$.

The other relevant feature is that the same procedure may be applied to obtain the solution for the uncoupled model. In fact, this solution has already been presented in the article [1].

3.3. Boundary conditions

In the context of the numerical procedure presented before, boundary conditions are imposed in Glimm's scheme in an approximated fashion. To see how it is implemented, the boundary conditions

$$P(x = 0, t) = P_o(t) \quad \text{and} \quad P(x = L, t) = P_o(t), \quad t \in [0, T], \tag{26.1}$$

$$\dot{u}(x = L, t) = 0 \quad \text{and} \quad \dot{u}(x = L, t) = 0, \quad t \in [0, T], \tag{26.2}$$

are considered for the problem in the next section.

In view of the change of variables (7), the boundary conditions (26.1) are expressed as

$$\rho_f c_f^2(D = 0, t)(\psi(x = 0, t) - 2v\phi(x = 0, t)) = P_o(t), \quad t \in [0, T],$$

$$\rho_f c_f^2(D = L, t)(\psi(x = L, t) - 2v\phi(x = L, t)) = P_o(t), \quad t \in [0, T].$$

For a generic time instant $t^{n+1} = t^n + \Delta t$, the boundary conditions (26.1) and (27) are imposed after advancing Δt in time in the procedure presented in Section 3.1, so that the above conditions are approximated by

© 1998 John Wiley & Sons, Ltd.

$$\begin{cases} \psi_1^{n+1} = \psi\left(0 < x < \dfrac{\Delta x}{2}, t^{n+1}\right) = P_o(t^{n+1})/(\varphi_f c_f^2(D_1^{n+1})) + 2v\phi_1^{n+1} \\ \dot{u}_1^{n+1} = \dot{u}\left(0 < x < \dfrac{\Delta x}{2}, t^{n+1}\right) = 0 \end{cases}$$

and

$$\begin{cases} \psi_{N+1}^{n+1} = \psi\left(L - \dfrac{\Delta x}{2} < x < L, t^{n+1}\right) = P_o(t^{n+1})/(\varphi_f c_f^2(D_{N+1}^{n+1})) + 2v\phi_{N+1}^{n+1} \\ \dot{u}_{N+1}^{n+1} = \dot{u}\left(L - \dfrac{\Delta x}{2} < x < L, t^{n+1}\right) = 0 \end{cases},$$

where $N\Delta x = L$, $D_1^{n+1} = D(0 < x < \Delta x/2, t^{n+1})$, $\phi_1^{n+1} = \phi(0 < x < \Delta x/2, t^{n+1})$, $D_{N+1}^{n+1} = D(L - \Delta x/2 < x < L, t^{n+1})$ and $\phi_{N+1}^{n+1} = \phi(L - \Delta x/2 < x < L, t^{n+1})$.

4. NUMERICAL EXAMPLE

As a first step to understanding the influence of the FSI coupling mechanisms on the structural integrity of piping systems, a relatively rigid pipe arrangement is considered. Numerical predictions of both models are then compared and analyzed.

Among other piping systems, reactor piping systems are known to be susceptible to viscoplastic deformations, due to combinations of transient pressure loadings and high operating temperatures. In the particular case of liquid metal fast breeder reactors, typical sources of pressure transients are the sodium–water reaction and a core disruptive accident. Both kinds of accidents can be well-represented by explosive pressure pulses of short duration [17,18].

Motivated by such accidents, the transient response of a single liquid-filled pipe of length L that is anchored and subjected to an impulsive pulse of pressure at its ends will be investigated. For this purpose, a senoidal-shaped pressure pulse will be considered so that the appropriate boundary conditions are

$$P(x = 0, t) = P(x = L, t) = P_o(t) = \begin{cases} P_m \sin(\pi/t^*) & \text{if } 0 \le t \le t^* \\ 0, & \text{if } t > t^* \end{cases},$$

where $P_m = 6$ MPa represents the pressure pulse amplitude and $t^* = 2$ ms is its duration. The pipe is a thin-walled tube filled with sodium at 600°C ($\rho_f = 832$ kg m^{-3} and $K = 2.31$ GPa). It is 10 m long, has an inside diameter of 73 mm and a wall thickness of 1.63 mm. The pipe material is an AISI 316 L stainless steel, the constitutive coefficients of which at 600°C are [7] $E = 130$ GPa, $v = 0.3$, $\sigma_p = 6$ MPa, $k = 150$ [GPa s^{-1}], $b = 80$ MPa, $d = 10$, $n = 12$, $a = 17$ GPa, $\varphi = 300$, $S_o = 2$ kPa, and $\varphi_t = 7800$ Kg m^{-3}.

As initial conditions for the simulation, the initial flow velocity is considered, with the pressure and axial stress fields at zero. In addition, it is assumed that the piping has never been subjected to plastic deformations, nor to any kind of degradation, so that the plastic strains, the damage and the other internal variables are set equal to zero before the accident takes place. In this context, the appropriate initial conditions are

© 1998 John Wiley & Sons, Ltd.

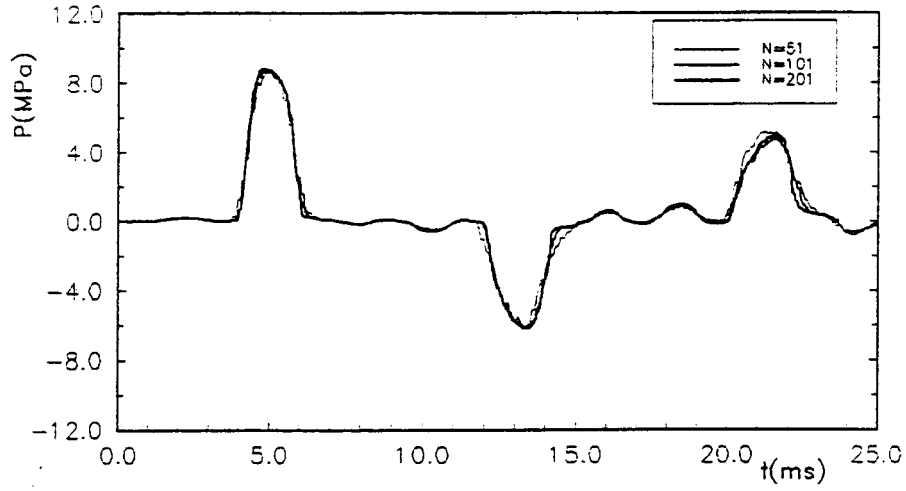

Figure 2. Pressure response versus time at $x/L = 0.5$ for different mesh sizes ($N = 51$, 101 and 201).

$$P(x, t=0) = 0, \qquad v(x, t=0) = 0, \quad x \in [0, L],$$
$$\varepsilon_\theta^a(x, t=0) = 0, \qquad \varepsilon_x^a(x, t=0) = 0, \qquad x \in [0, L],$$
$$\boldsymbol{\beta}(x, t=0) = 0, \qquad D(x, t=0) = 0, \quad x \in [0, L].$$

For the coupled model, apart from the initial conditions presented before, consider the conditions

$$\sigma_x(x, t=0) = 0, \qquad \dot{u}(x, t=0) = 0, \quad x \in [0, L],$$
$$\dot{u}(x=0, t) = 0, \qquad \dot{u}(x=L, t) = 0, \quad x \in [0, T].$$

Before presenting some interesting results, it is important to mention that a number of numerical experiments have been performed to check the precision and accuracy of the proposed numerical technique. Convergence tests have been carried out for the elasto-viscoplastic behavior by considering different mesh sizes ($N = 51$, 101, 201). The results obtained are depicted in Figure 2, which shows the pressure as a function of the time at the spatial position $x/L = 0.5$. It can be seen, from $N = 51$ to 101 the solutions tend to converge to that with $N = 201$. With $N = 101$ and 201 there is no significant differences between the responses.

In what follows, the transient response of the system will be analyzed based upon both coupled and uncoupled models.

Pressure response as a function of time and position along the pipe is illustrated in Figure 3 for both uncoupled (Figure 3a) and coupled (Figure 3b) models. After $t = 0$, pressure pulses generated at $x = 0$ and $x = L$ move towards the pipe midpoint where superposition takes place. Afterwards, these pulses will be reflected at pipe's ends until steady state has been reached (Figure 3b) or piping rupture has occurred (Figure 3a). According to the predictions of the uncoupled model (Figure 3a), piping rupture takes place at $t = 5.4$ ms when pressure pulses are superimposed for the first time. On the other hand, for the coupled model (Figure 3b), even after the third interaction of the pressure pulses in the midpoint of the tube, piping rupture has not occurred. In addition to pressure pulse attenuation, it is interesting to note the presence of second-order perturbations in the response of the coupled model (Figure 3b) after $t = 10$ ms due to the Poisson coupling.

© 1998 John Wiley & Sons, Ltd.

To obtain a better idea of the damage evolution along the pipe according to both models, Figure 4 (for the uncoupled model) and Figure 5 (for the coupled model) show the spatial pressure (left column) and damage (right column) fields at different time instants. Since pressure amplitude of each individual pulse is not capable to induce pipe wall plastic deformations, it can be observed that for both models, pressure pulses propagate without suffering attenuation or dispersion until $t \simeq 5$ ms. Thus from $t = 0$ ms to that instant, there has been no damage evolution, as it can be seen in the curves $D \times x/L$ for $t = 2.95$ and 3.93 ms in Figures 4 and 5.

At $t \simeq 5$ ms, when pressure pulse superposition occurs for the first time, the resulting pressure amplitude induces (in both models, Figures 4 and 5) a damage of $\approx D = 0.1$ near the midpoint of the pipe. It should be noticed that, due to the viscoplastic behavior, the resulting pressure amplitude (of ≈ 8 MPa) is less than the sum of the amplitudes of the pulses. After $t \simeq 5$ ms, the damage evolution predictions of the uncoupled and coupled models become different. It can be observed that for the uncoupled model (Figure 4) the damage jumps quickly from $D = 0.1$ at $t = 4.91$ ms to $D = 0.85$ at $t = 5.37$ ms. For the coupled model (Figure 5), however, the damage increases from $D = 0.1$ to 0.25 during the same time interval.

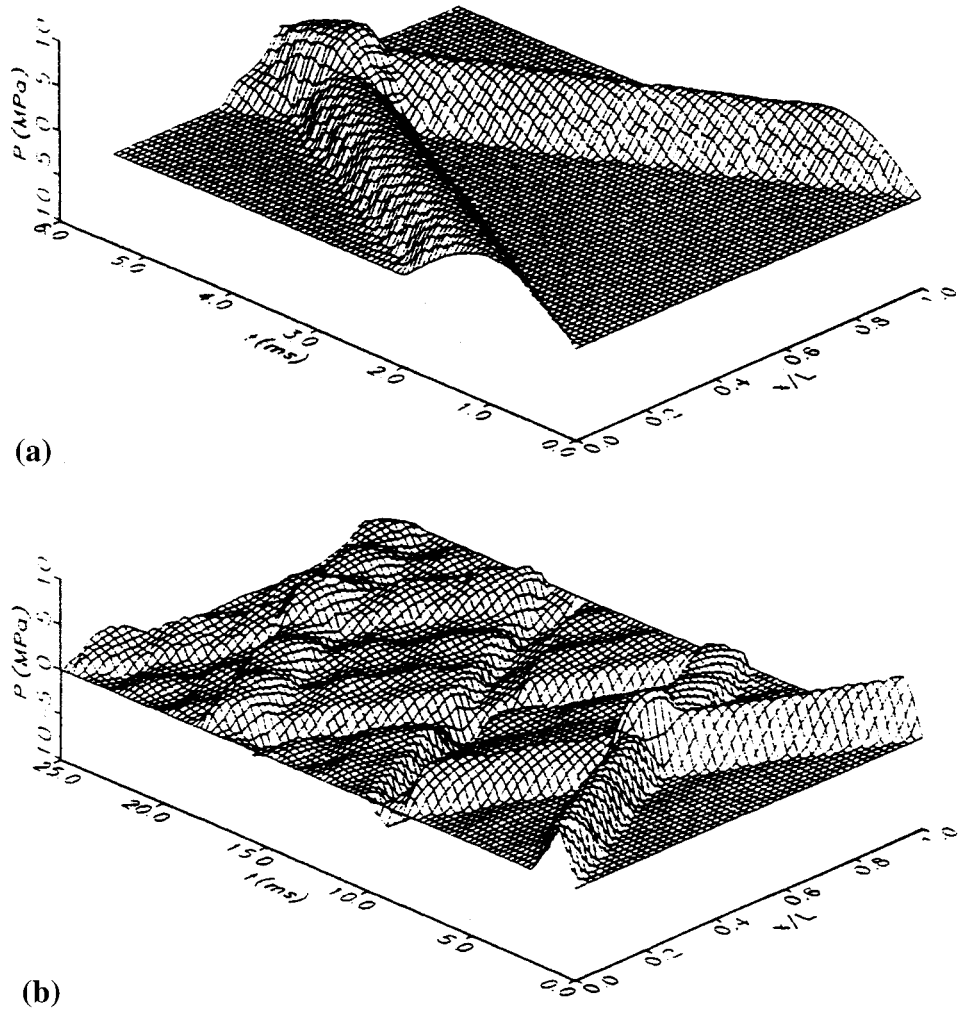

Figure 3. Pressure 3D response. a) Uncoupled model. b) Coupled model.

© 1998 John Wiley & Sons, Ltd.

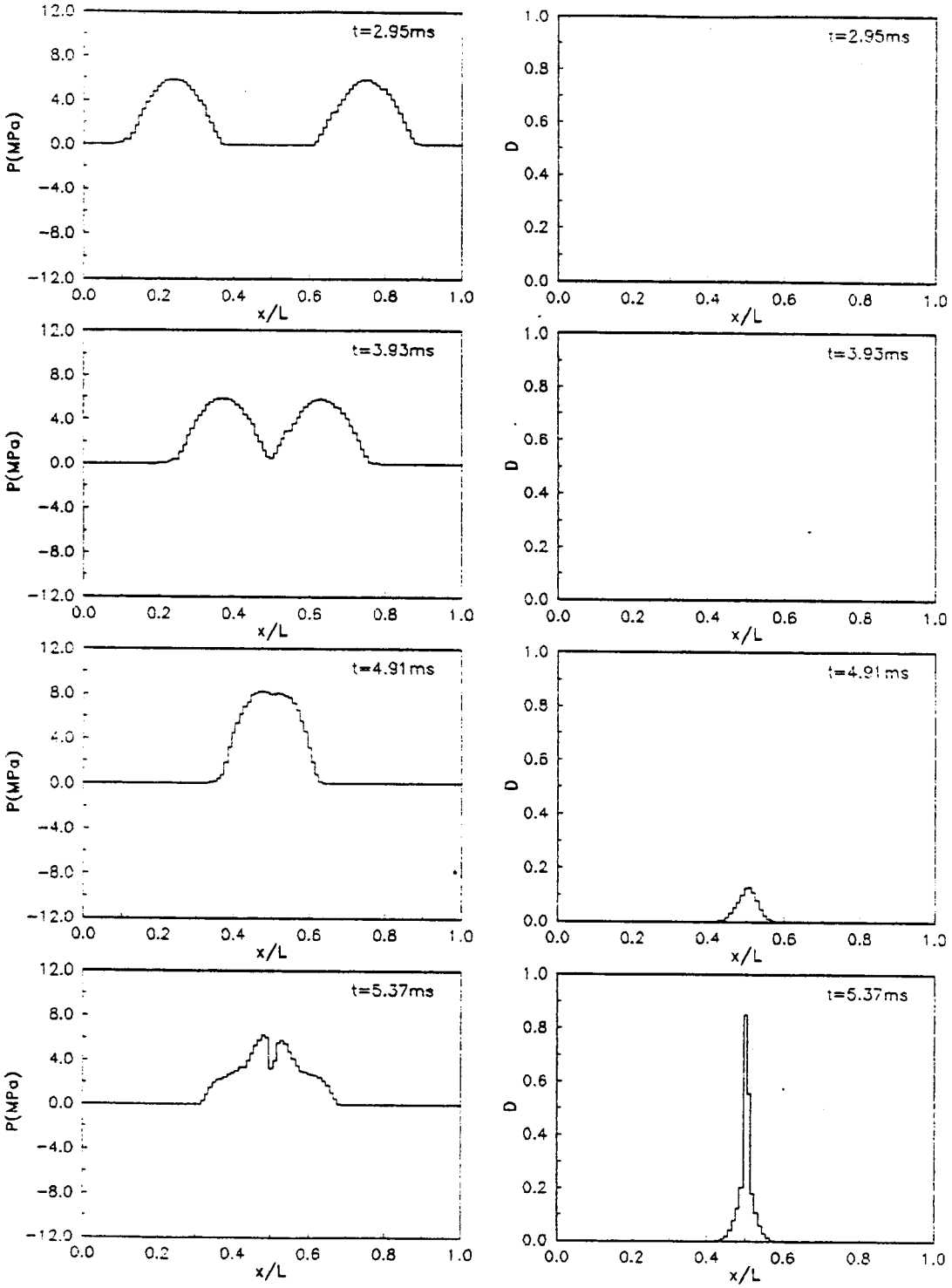

Figure 4. Pressure and damage versus position along the pipe for several time instants. Uncoupled model.

© 1998 John Wiley & Sons, Ltd.

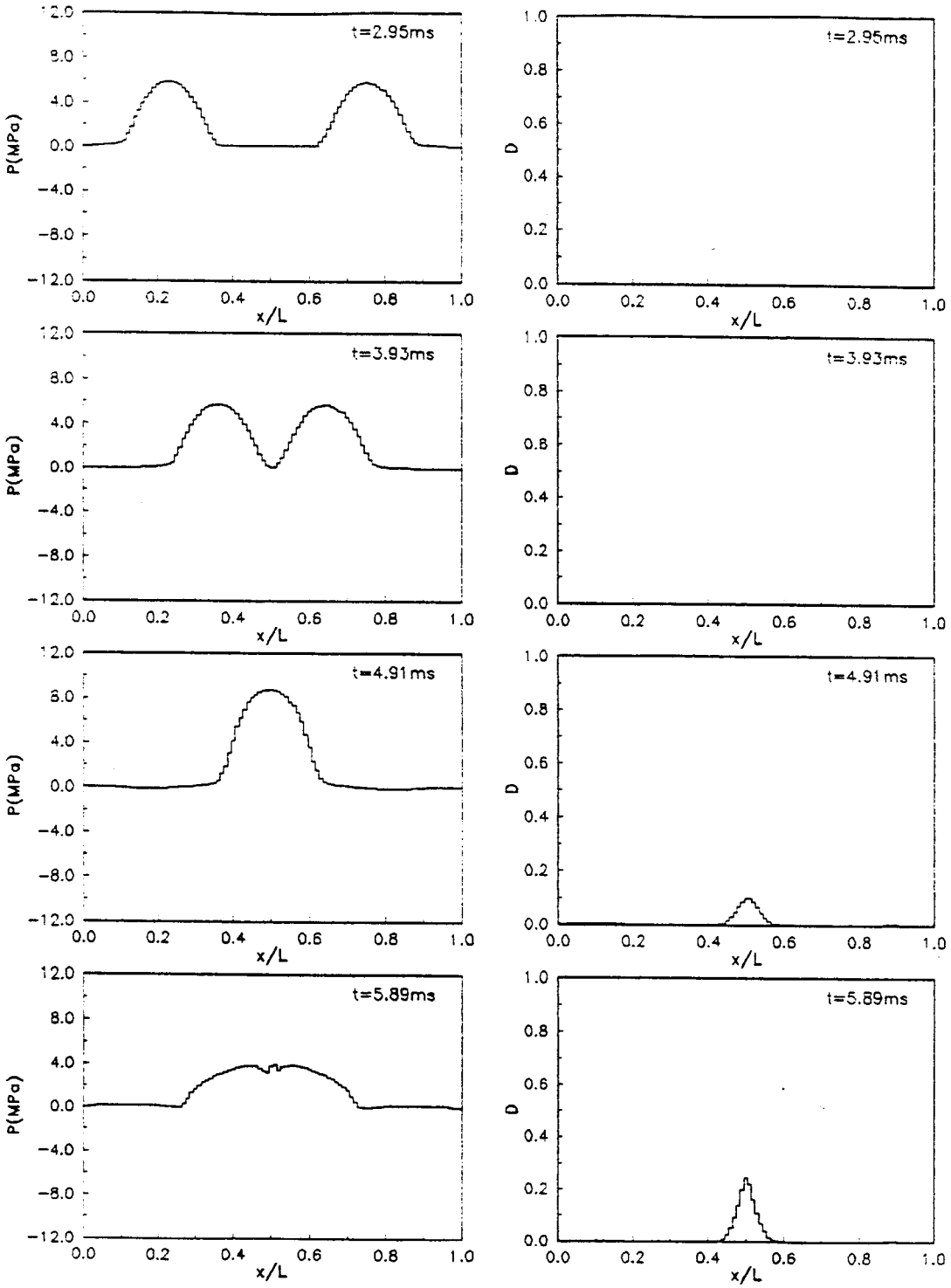

Figure 5. Pressure and damage versus position along the pipe for several time instants. Coupled model.

© 1998 John Wiley & Sons, Ltd.

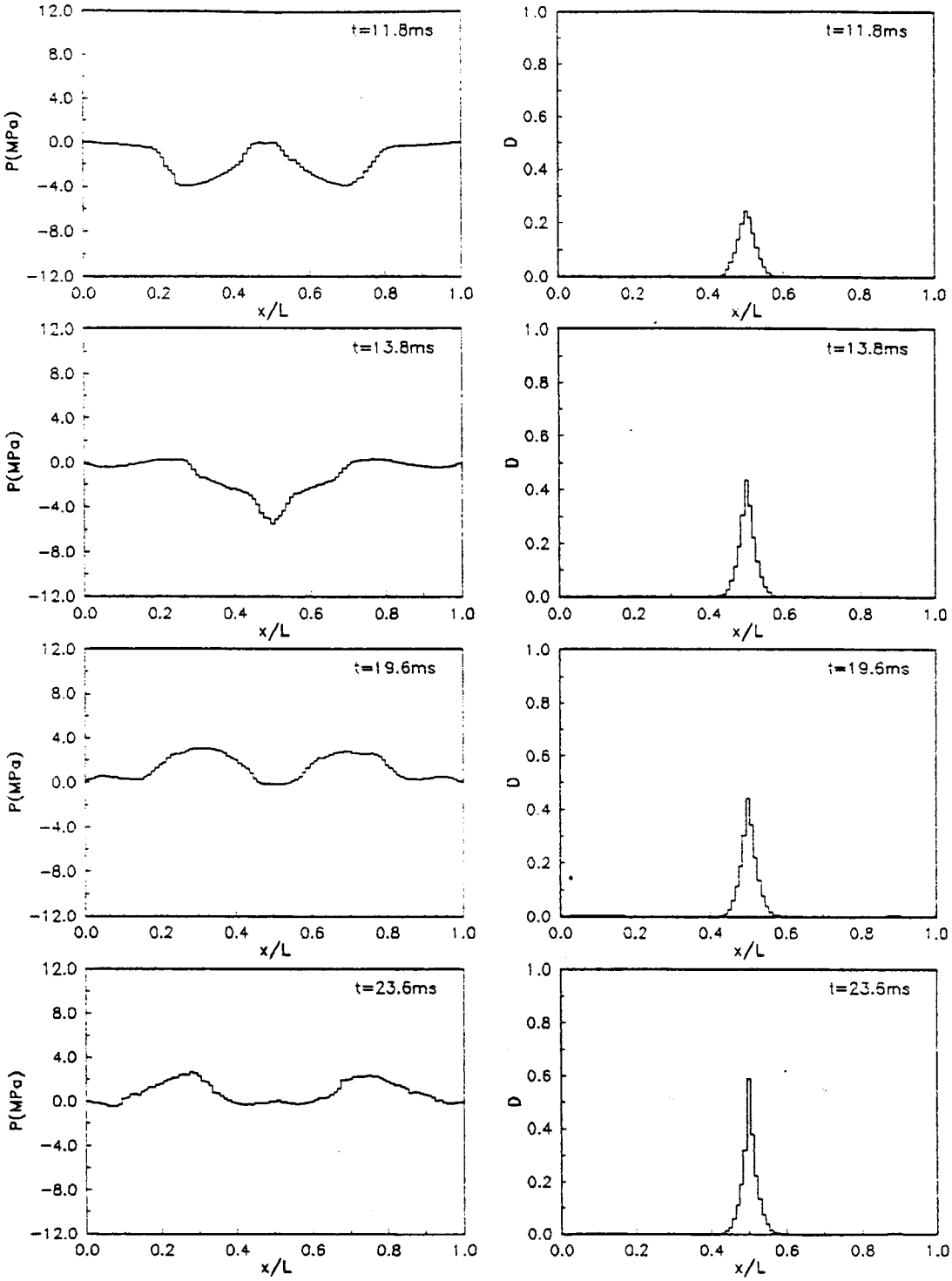

Figure 6. Pressure and damage versus position along the pipe for several time instants. Coupled model. (Continued from Figure 5).

© 1998 John Wiley & Sons, Ltd.

The remaining sequence of damage and pressure fields shown in Figure 5 is depicted in Figure 6. It can be seen in Figure 6 that the damage evolution takes place more slowly than that predicted by the uncoupled model.

The piping only experiences significant damage after 23 ms. However, the cumulative damage is not enough to induce piping rupture. When compared with the uncoupled model, the coupled model predicts a gradual damage evolution since it considers an additional direction (the axial direction) to dissipate the strain energy.

5. CONCLUSIONS

Two models (a coupled and an uncoupled), along with a numerical procedure based upon Glimm's scheme and the operator splitting technique, have been proposed to predict the structural integrity of liquid transmission lines subjected to hydraulic transients. The coupled model takes into account the axial FSI, whereas the uncoupled one refers to an extension of the well-known waterhammer formulation. By comparing the numerical results of both models, it has been shown that the uncoupled model overestimates the level of degradation in the pipe. Such a conservative prediction, along with its simplicity, enables the uncoupled model to be used for preliminary integrity analyses of relatively rigid piping structures. Based on previous work [5], similar results should not be expected for flexible piping arrangements. Current research is underway to investigate this in detail.

ACKNOWLEDGMENTS

The research reported in this work was developed at the Laboratory of Theoretical and Applied Mechanics (LMTA) of the Universidade Federal Fluminense (UFF) and was financially supported by grants CNPq 301.323/94-1 and 523.991/96-7 and FAPERJ 170.279/95.

APPENDIX A. EVOLUTION LAWS FOR THE DAMAGEABLE ELASTO-VISCOPLASTIC BEHAVIOR

The expressions of the functions $(\mathbf{g}, h, \ell)$ which characterize the evolution laws (Equations (4.2)–(4.4)) are

$$\mathbf{g} = \frac{3}{2}\frac{1}{(1-D)}\left\langle \frac{f}{k(1-D)} \right\rangle^{n} \frac{(\boldsymbol{\sigma}+\mathbf{B}^{\mathbf{c}})_{\mathrm{dev}}}{J(\boldsymbol{\sigma}+\mathbf{B}^{\mathbf{c}})},$$

$$h = \frac{B^{D}}{S_o}\frac{1}{(1-D)}\left\langle \frac{f}{k(1-D)} \right\rangle^{n},$$

$$\ell = \left(\left\langle \frac{f}{k(1-D)} \right\rangle^{n}, \mathbf{g} - \frac{\varphi\, \mathbf{B}^{\mathbf{c}} h S_o}{a B^{D}} \right),$$

where $\langle x \rangle = \max\{0, x\}$,

$$f = J(\boldsymbol{\sigma}+\mathbf{B}^{\mathbf{c}}) + B^{p} - \sigma_p(1-D),$$

$$J(\boldsymbol{\sigma}+\mathbf{B}^{\mathbf{c}}) = \left(\frac{3}{2}(\boldsymbol{\sigma}+\mathbf{B}^{\mathbf{c}})_{\mathrm{dev}}(\boldsymbol{\sigma}+\mathbf{B}^{\mathbf{c}})_{\mathrm{dev}} \right)^{1/2},$$

© 1998 John Wiley & Sons, Ltd.

$$B^p = -b(1-\exp(-dp)),$$

$$\mathbf{B}^{\mathbf{c}} = -a\mathbf{c},$$

$$B^D = \frac{1}{2}(\mathbf{C}(\boldsymbol{\varepsilon}-\boldsymbol{\varepsilon}^{\mathbf{a}}))\cdot(\boldsymbol{\varepsilon}-\boldsymbol{\varepsilon}^{\mathbf{a}}),$$

with $(\boldsymbol{\sigma}+\mathbf{B}^{\mathbf{c}})_{\text{dev}}$ being the deviatoric part of $(\boldsymbol{\sigma}+\mathbf{B}^{\mathbf{c}})$ and a, b, d, k, n, σ_p, φ and S_o are the material parameters.

REFERENCES

1. F.B. Freitas Rachid, H.S. Costa Mattos and R.M. Saldanha da Gama, 'Modelling of hydraulic transients in damageable elasto-viscoplastic piping systems', *Appl. Math. Modelling*, **18**, 207–215 (1994).
2. F.B. Freitas Rachid and H.S. Costa Mattos, 'Pressure transients in damageable elasto-plastic pipes', *Proc. 1995 Joint ASME/JSME Pressure Vessel and Piping Conf.*, Honolulu, USA, **301**, 31–40 (1995).
3. F.B. Freitas Rachid and H.S. Costa Mattos, 'Modelling the damage induced by pressure transients in elasto-plastic pipes', *Meccanica*, (to appear) (1997).
4. D.C. Wiggert, 'Coupled transient flow and structural motion in liquid-filled piping systems: a survey', *Proc. ASME Pressure Vessels and Piping Conf.*, Chicago, USA, 1986, 86-PVP-4.
5. F.B. Freitas Rachid, H.S. Costa Mattos and S. Stuckenbruck, 'Fluid–structure interaction in elasto-viscoplastic piping systems', *Proc. 1st ASME/JSME Joint Fluids Eng. Conf.*, Portland, USA, 1991, pp. 65–73.
6. E.B. Wylie and V.L. Streeter, *Fluid Transients in Systems*, Prentice Hall, New York, 1993.
7. J. Lemaitre and J.L. Chaboche, *Mechanics of Solid Materials*, Cambridge University Press, Cambridge, 1990.
8. J.S. Walker and J.N. Philips, 'Pulse propagation in fluid-filled tubes', *ASME J. Appl. Mech.*, **3**, 31–35 (1977).
9. F.B. Freitas Rachid and H.S. Costa Mattos, 'On the modelling of pressure transients in damageable pipings', *RBCM J. Brazilian Soc. Mech. Sci.*, **15**, 332–341 (1993).
10. D. Marchesin and P.J. Paes-Leme, 'Shocks in gas pipelines', *SIAM J. Sci. Stat. Comput.*, **4**, 105–116 (1983).
11. G.A. Sod, 'A numerical study of a converging cylindrical shock', *J. Fluid Mech.*, **83**, 785–794 (1977).
12. J. Glimm, 'Solutions in the large for nonlinear hyperbolic systems', *Commum. Pure Appl. Math.*, **18**, 697–715 (1965).
13. A.J. Chorin, 'Random choice solutions of hyperbolic systems', *J. Comput. Phys.*, **22**, 517–553 (1976).
14. P. Collela, 'Glimm's method for gas dynamics', *SIAM J. Sci. Stat. Comput.*, **3**, 76–110 (1982).
15. P.L. Roe, 'Approximate Riemann solvers, parameters, vectors and difference schemes', *J. Comput. Phys.*, **43**, 357–372 (1981).
16. J. Smoller, *Shock Waves and Reaction–Diffusion Equations*, Springer, New York, 1983.
17. G.L. Fox and D. Stepnewski, 'Pressure wave transmission in a fluid contained in a plastically deforming pipe', *J. Pressure Vessel Tech.*, **96**, 258–262 (1974).
18. C.K. Youngdahl and C.A. Kot, 'Effect of plastic deformation of piping on fluid-transient propagation', *Nucl. Eng. Des.*, **35**, 315–325 (1975).

© 1998 John Wiley & Sons, Ltd.